PCCP

Accepted Manuscript

ROYAL SOCIETY OF CHEMISTRY

rsc.li/pccp

View Article Online
DOI: 10.1039/C8CP05330H

Journal Name

ARTICLE

Operando Investigations of Lithiation and Delithiation Processes in the $BiVO_4$ Anode Material

Received 00th January 20xx,
Accepted 00th January 20xx

DOI: 10.1039/x0xx00000x

www.rsc.org/

Amund Ruud, [a] Jonas Sottmann, *[a] Ponniah Vajeeston [a] and Helmer Fjellvåg *[a]

$BiVO_4$ undergoes a series of conversion and alloying reactions as anode material in lithium ion batteries. The current work demonstrates a charge capacity of 485 mAh g^{-1} after 50 cycles in a voltage range of 0 – 2.00 V (graphite 372 mAh g^{-1} theoretically). An exceptionally high volumetric capacity makes $BiVO_4$ suitable for compact applications (volumetric capacity of 3984 mAh cm^{-3} for $BiVO_4$ in comparison to 756 mAh cm^{-3} for graphite theoretically). Reaction steps and electronic transformations have been identified by *operando* quasi simultaneous synchrotron x-ray diffraction and absorption spectroscopy studies. An irreversible reaction step occurs for the Bi^{3+}/Bi^0 redox pair, whereas reversible mechanisms are found for V^{5+}/V^{3+} and Bi^0/Bi^{3-} redox pairs. The proposed mechanisms are supported by density functional theory (DFT) calculations.

Introduction

Lithium ion batteries (LIBs) are conquering the rapidly expanding market for electric transportation. Despite the fact that LIB technology is becoming more mature, intensive research is still devoted to identify electrode materials with higher gravimetric and volumetric capacities for next generation LIBs. Today, graphite is the most widely used anode material (gravimetric capacity of 372 mAh g^{-1} and volumetric capacity of 756 mAh cm^{-3} for LiC_6). With respect to oxide anodes, $Li_4Ti_5O_{12}$ is commercially available, albeit having a moderate theoretical capacity of 175 mAh g^{-1} (volumetric capacity 610 mAh cm^{-3}). Still $Li_4Ti_5O_{12}$ is technologically competitive in cases where extended cyclability and high charge and discharge rates are of prime importance.[1]

Among anode materials explored at the research stage, silicon holds promise for implementation but reversibility suffers due to volume expansions during lithium alloying (note: small silicon additives are now used in commercial anodes, improving specific capacity). Transition metal oxide (TMO) and more recently, mixed transition metal oxide (MTMO) anodes are launched with prospects on large volumetric capacities compared to today's anode technologies.[2-5] An example of an MTMO is $CoSnO_3$ where complete reduction of both Co and Sn, and further alloying of Sn with Li, results in very high specific capacity (theoretical capacity of 1188 mAh g^{-1} for 10 Li per formula unit).[6] Typically such MTMOs suffer from major capacity fading during the first cycle as well as reduced coulombic efficiency during subsequent cycling. The latter may to some extent be improved by nanoscaling and carbon additives. Recently, fern architectured $BiVO_4$ was reported as anode for LIBs by Dubal *et al*.[7] Although a considerable capacity loss occurred during the first cycle, a reversible capacity of 600 mAh g^{-1} was obtained at 1.1 A g^{-1} for 200 cycles (theoretical capacity 745 mAh g^{-1} for 9Li per $BiVO_4$; volumetric capacity of 3984 mAh cm^{-3}).[7, 8] Furthermore, $BiVO_4$ also shows great promise as sodium ion battery anode.[9, 10]

For exploring property – performance relationships of state-of-the-art battery materials as well as for emerging anode and cathode systems, detailed insight provided by *operando* methods are crucial. In this respect, data collected *post mortem* provide results based on the outcome of processes that have taken place in a battery (like phase transitions, intercalation, SEI formation, etc.), but only *operando* methods give true insight during the very cycling operations without introducing unwanted effects (oxidation, changes caused by handling or storage, etc.). Several *operando* methods are now at hand; x-ray based techniques (synchrotron x-ray absorption, diffraction and tomography) neutron diffraction, scanning and transmission electron microscopy, etc.[11, 12] This includes tools like pair distribution function (PDF) analysis and mass spectroscopy (MS) studies of evolved gas.[13]

In the current paper, we report on *operando* synchrotron X-ray absorption and diffraction (XANES and SXRD) studies of $BiVO_4$ as a LIB anode that shows good cyclability and retained 70 % charge capacity after 50 cycles. The *operando* data allowed us to unravel the lithiation and delithiation reactions during charge and discharge. We address differences between these two processes and discuss the effect of the applied voltage window by comparing *operando* data for the 0.01 – 2.0 V and 0.01 – 2.5 V voltage ranges. The experimental observations for the crystalline phases and their amorphization, are complemented by effects observed in XANES spectra, and supplemented with DFT simulations of the energetics of the involved reactions.

Experimental

Synthesis. The oxide – carbon composite $BiVO_4$:C was prepared by milling commercial $BiVO_4$ (99.9 %, Alfa Aesar) powder and conductive carbon black (C, Timcal Super P) in a mass ratio of 7:3 under Ar atmosphere. A Fritsch Mini-Mill Pulverisette 23 was used at 50 Hz with a ball-to-powder ratio of 10:1 for 20 min. The grinding balls and bowls were made of steel. All handling,

[a] Center for Materials Sciences and Nanotechnology, Department of Chemistry, University of Oslo, P.O. Box 1033 Blindern, N-0315 Oslo, NorwayElectronic Supplementary Information (ESI) available: [details of any supplementary information available should be included here]. See DOI: 10.1039/x0xx00000x

DOI: 10.1039/C8CP05330H

including electrode synthesis, was done in a glove box under Ar atmosphere (99.999% purity).

Structural Characterization. Products of $BiVO_4$ after ball milling were imaged with a Hitachi SU8230 cold-field emission scanning electron microscope (SEM; see Fig. S 1); acceleration voltage 10 kV, beam current 10 µA at a working distance of approximately 9 mm. A Bruker D8 Advance, CuKα1 (λ = 1.54059 Å) radiation, equipped with LynxEye XE detector and Ge (111) monochromator, was used to collect diffraction data for crystal structure refinements of pristine $BiVO_4$ by means of the TOPAS V5 (Bruker AXS) software.[14]

Electrochemical Characterization. Electrode preparation was performed in a glove box (MBraun) with O2 and H2O levels < 0.1 ppm under Ar atmosphere (99.999 %). The working electrode was prepared by spreading a slurry of 70 wt % BiVO4:C, 10 wt % conductive carbon black (Super P, Timcal) and 20 wt % poly(acrylic acid) binder (PAA, Sigma Aldrich) dissolved in ethanol on a Cu foil. The electrodes were dried under vacuum at 60 °C overnight, and thereafter stamped into discs with a mass loading of active material of about 1 mg cm-2. The battery was assembled in (CR2032) coin cells in the glove box. The working electrode was separated from the Li metal counter electrode by electrolyte soaked glass fibres (GF/C, Whatman). A 1 M solution of LiPF6 in ethylene carbonate/diethyl carbonate (EC/DEC, 1:1 in wt) (LP30) was used as electrolyte. Galvanostatic cycling was carried out at a current of 150 mA g-1 (equal to a dis-/charge rate of about C/6.6 estimated from a theoretical capacity of 996 mAh g^{-1} calculated from a 12 electron reaction) using a Bat-Small battery cycler (Astrol). In the previous studies by Dubal *et al.* cycling was done in the regime 0.01 – 3.00 V.[8] In our study we investigated two ranges 0.01 - 2.00 V and 0.01 – 2.50 V. The range 0.01 – 2.00 V resulted in sufficient oxidation of the anode for achieving reversible cycling. The range 0.01 – 2.50 V was included to check for possible effects caused by higher oxidation potentials.

Operando XRD and XANES. *Operando* synchrotron X-ray diffraction (SXRD) and x-ray absorption near edge spectroscopy (XANES) data were collected at the Swiss-Norwegian Beam Line (SNBL), BM01B, at ESRF, Grenoble. Bismuth L3 edge XANES data were measured in transmission mode using a Si(111) channel-cut monochromator. The second crystal was detuned to reduce higher harmonics. The XANES data were analyzed using ATHENA for absorption edge determination and spectrum normalization to an edge jump of one unity.[15] The absorption edge position was determined as maximum of the first derivative. An Ir foil (the Ir L1 edge at 13419 eV is observed at the same position as the Bi L3 edge) was used as reference, calibrated by the maximum value of the 1st derivative. The electrochemical cycling for the *operando* studies was performed in Swagelok type electrochemical cells with Kapton windows as earlier described.[16] The *operando* battery cell assembly is identical to that of the home lab coin cells described above. The first 1.5 galvanostatic cycles were followed *operando*. The applied current was chosen to let each dis-/charge to take approximately 10 h. Collection of XANES data (2 min per scan) followed by SXRD data using a Dexela 2923 CMOS two-dimensional detector (1 min per scan) was performed in sequence for several cells mounted in an automatized sample changer with 12 positions.[16]

Computational details. Total energies were calculated by the projected-augmented plane-wave (PAW) implementation of the Vienna *ab initio* simulation package (VASP).[17, 18] All calculations were made with the Perdew, Burke and Ernzerhof (PBE) exchange correlation functional.[19] Ground-state geometries were determined by minimizing stresses and Hellman-Feynman forces using the conjugate-gradient algorithm with force convergence < 10^{-3}eV $Å^{-1}$. Brillouin zone integration was performed with a Gaussian broadening of 0.1 eV during all relaxations. It was found that 2050 **k**-points per atom in the whole Brillouin zone for the structure with a 600 eV plane-wave cut-off are sufficient to ensure good accuracy in the computed results. The iterative relaxation of atomic positions was run until the change in total energy between successive steps was less than 1 meV per cell. For the reaction energy calculation the following compounds (and polymorphs) were evaluated: Li (Im-3m), Bi (R-3m), Bi_2O_3 ($P2_1/c$), LiBi (P4/mmm), Li_3Bi ($P6_3/mmc$), VO (R-3m), VO_2 ($P4_2/mnm$), V_2O_5 (Pmnm), $BiVO_4$ (I41/amd), LiBi (P4/mmm), Li_3Bi (Fm-3m), Li_3VO_4 ($Pmn2_1$), Li_3BiO_3 (Pccn), BiO (R3m), $LiVO_2$ (R-3m), Li_2O (Fm-3m), LiV_2O_5 (Pnma), Bi_2O_3 ($P2_1/c$), Li_2O_2 (P63/mmc), $LiBiO_2$ (Ibam), $LiBiO_3$ (Pccn), Li_3BiO_4 ($P4_2/mnm$), BiO_2 (Fm-3m), Li_4VO_4 (P-1), Li_3VO_4 ($Pmn2_1$), LiV_3O_8 ($P2_1/m$), and $Li_2V_6O_{13}$ (C2/m). The structural data were taken from the ICSD database.[20] In this work the total energy difference between the reactants and products is represented as the reaction enthalpies. Voltages were calculated according to the two-phase coexistence method.[21]

Results

Structural and electrochemical characterization. Bismuth vanadate, $BiVO_4$, crystallizes in space group C12/c1 and contains isolated VO_4 tetrahedra connected by distorted BiO_8 dodecahedrons, see Fig. 1, as confirmed by Rietveld refinements of current XRD data, see Fig. S 1 and Table S 1. The Bi(III) and V(V) cations in $BiVO_4$ can be reduced during reaction with lithium, with Bi(-III) and V(0) as theoretical end points.

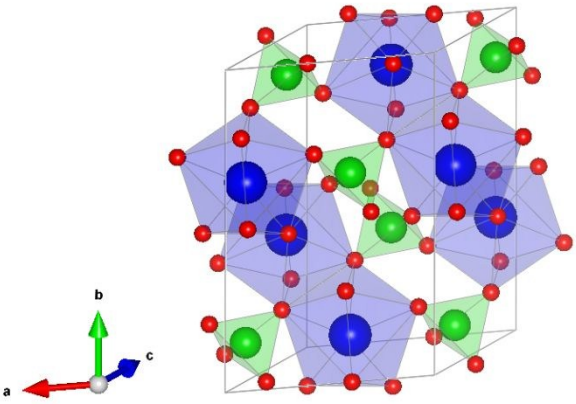

Fig. 1. Crystal structure of $BiVO_4$. Blue, green and red spheres represent Bi, V, and O atoms respectively.[22] Coordination polyhedral indicated for Bi and V.

The galvanostatic profile of $BiVO_4$ cycled in the range of 0.01 - 2.50 V along with the specific dis-/charge capacity against cycle number for 0.01 – 2.00 V and 0.01 – 2.50 V are reported in Fig. 2 a) and b), respectively. For the 1st discharge, i.e. the lithiation, the specific capacity for $BiVO_4$ is 973 mAh g^{-1} for the voltage range 0.01-2.00 V and 1121 mAh g^{-1} for the voltage range 0.01 - 2.50 V (Note: for a perfect system the 1st discharge capacity should be similar for both voltage ranges). A large plateau during 1st discharge is seen at around 1.75 V, a feature that was not reproduced in consecutive cycles. The capacity is lowered to 570 (39 % loss) and 696 mAh g^{-1} (38 % loss), respectively, during the 1st charge, i.e. delithiation, as shown in Fig. 2b. After 50 cycles the discharge capacity becomes 431 and 485 mAh g^{-1} for the voltage ranges 0.01 – 2.00 V and 0.01 - 2.50 V, respectively. The more narrow voltage window gives a somewhat lower capacity, however, on the other hand a more stable cycling.

View Article Online
DOI: 10.1039/C8CP05730H

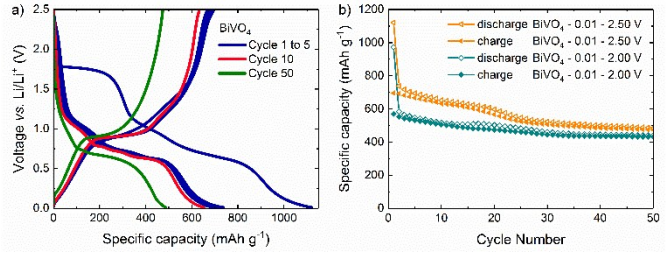

Fig. 2. Galvanostatic measurements of $BiVO_4$; (a) potential vs Li/Li$^+$ (V) versus specific capacity (mAh g^{-1}) for cycle number 1 to 5 (blue), 10 (red) and 50 (green) cycled in the range 0.01 - 2.5 V; (b) Specific dis-/charge capacity (mAh g^{-1}) from cycling studies in the ranges 0.01 – 2 (cyan) and 0.01 - 2.5 V (orange) at a current density of 150 mA g^{-1}.

Differential capacity plots are shown for the 1st, 2nd and 5th cycle in Fig. 3 for the voltage ranges a) 0.01 – 2.0 V and b) 0.01 – 2.5 V. The large anodic peak at about 1.75 V for both ranges is unique to the 1st discharge. Less well-defined anodic peaks occur at about 1.00, 0.70 and 0.65 V, whereas cathodic peaks are observed at about 0.89 V.

During the 2nd discharge the anodic reactions at about 0.73 and 0.62 V shift slightly to higher voltages, appearing at 0.74 and 0.64 V during the 5th discharge. During the 2nd charge there are two close cathodic peaks at about 0.86 and 0.90 V. In the 5th charge only one large cathodic peak is observed at about 0.90 V.[23] By comparing the data in Fig. 3, it is evident that all peaks, omitting the 1st discharge at 1.75 V, become narrower and larger in magnitude on progressive cycling. In addition, for the cycling range 0.01 – 2.5 V one small anodic peak at 0.8 V and a cathodic peak at 0.87 V appears for the 5th cycle. The two sharp anodic peaks, at 0.74 and 0.64 V, occur at potentials comparable to what Xianming *et al.* reported,[23] and relates to the reactions: 3Li + Bi ↔ 2Li+ LiBi ↔ Li_3Bi. Xianming *et al.* reported this two step lithiation process to be fully reversible. However, for the present anode this is just evidenced by two cathodic peaks for the 2nd cycle, at 0.86 and 0.90 V.

Redox reactions that involve vanadium are indicated by the broad anodic peak at about 1.00 V and the cathodic peak at 1.30 V. These potentials are comparable to what was reported by Liao *et al.* for cycling studies of Li_3VO_4.[24]

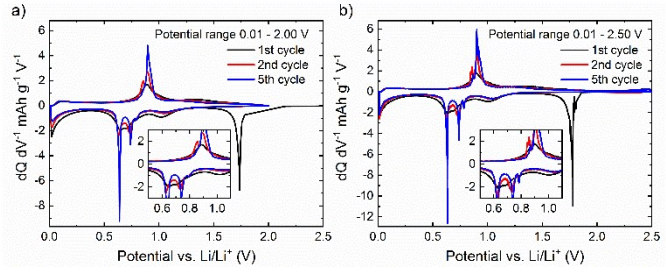

Fig. 3. dQ dV^{-1} (mAh g^{-1} V^{-1}) as function of potential vs. Li/Li$^+$ for 1st (black), 2nd (red) and 5th (blue) galvanostatic cycling of $BiVO_4$ in the range (a) 0 – 2 V; and (b) 0 – 2.5 V. Insets highlights the voltage region 0.5 – 1.10 V

Operando XANES and SXRD

The chemical state of bismuth and the structural properties of $BiVO_4$ were followed during first 1.5 cycles by *operando* SXRD and XANES. The large background at low scattering angles is due to amorphous contributions from separator, kapton windows and electrolyte. As shown in Fig. 4 the crystallinity of $BiVO_4$ is irreversibly lost during the 1st discharge within the plateau at around 1.75 V. Bragg reflections from metallic bismuth appears for the last three scans of the 1st charge and are further detected during the first three scans of the 2nd discharge. During the 2nd discharge, metallic Bi (R-3m h) alloys to form LiBi (P4/mmm) and finally Li_3Bi (Fm-3m). The reflections are weak; nevertheless, their appearance is well documented. All peaks are broad, indicative of small crystallite sizes (Fig. S 3).

The fourth scan (orange, Fig. 4) collected during the 2nd discharge, clearly shows (101) from LiBi at $2\theta \approx 11°$. In the subsequent scans, also Bragg peaks of Li_3Bi appear, insert shows (111) from Li_3Bi at $2\theta \approx 7.5°$, Fig. 4. The observed reaction sequence 3Li + Bi → 2Li + LiBi → Li_3Bi is consistent with the two step mechanism suggested based on the peaks at 0.73 and 0.62 V in the dQ dV^{-1} curves (Fig. 3). The Bi, LiBi and Li_3Bi diffraction peaks remain weak compared to the Bragg reflections initially observed for $BiVO_4$ (inset in Fig. 4 and Fig. S 3). This indicates that the electrochemical reactions take place mainly between amorphous or nanocrystalline Li-Bi and Li-V-O phases.

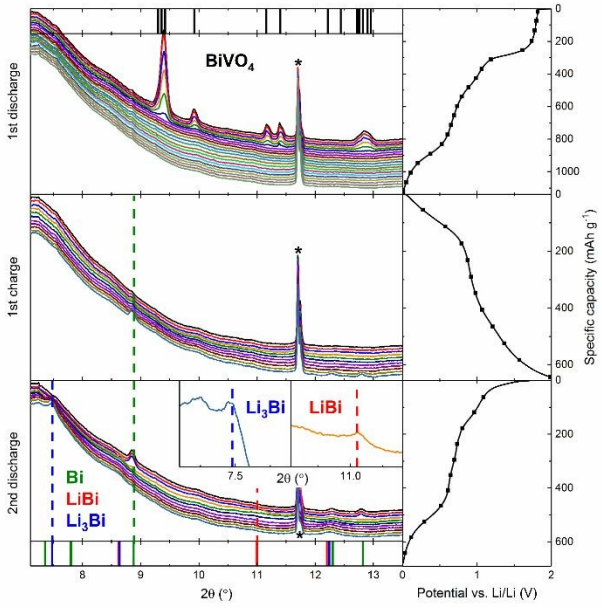

Fig. 4. *Operando* SXRD of $BiVO_4$ for 1st discharge, 1st charge and 2nd discharge (left), with corresponding cycling data (right). The shown diffractograms were collected at potential/capacity conditions marked ■. Downwards cascading diffractograms start from the initial state in each sequence with subsequent scans during cycling. Top bars (black) indicate Bragg reflections of $BiVO_4$ whereas bottom bars similarly indicate Bi (green), LiBi (red) and Li_3Bi (blue) phases. Insets in 2nd discharge plot show unique reflections for Li_3Bi (left) and LiBi (right) respectively. Asterix * marks peaks from metallic lithium used as anode. Wavelength λ = 0.5053 Å.

Normalized XANES spectra and the 1st derivatives of the Bi L3 edge for the first 1.5 cycles are shown in Fig. S 4. During the 1st discharge one notices a loss of signal for the first absorption peak at about 13434 eV as indicated by the downward arrow, Fig. S 4 top left panel. Simultaneously, the Bi L3 edge shifts towards lower energies, associated with Bi reduction. The edge shift is clearly visible in the 1st derivative curves, Fig. S 4 top right panel. Middle and bottom panel shows subsequent reversibility during cycling. An isosbetic point at 13416 eV is seen for both the 1st charge and 2nd discharge, indicating at least a two-phase reaction. The data quality is not sufficient for a more detailed analysis.

The extracted peak position from the 1st derivative XAS spectra allowed us to correlate voltage profile with the Bi L3 absorption energies as a function of specific capacity during the dis-/charge processes, Fig. 5. For the initial plateau at about 1.75 V, a clear shift in the Bi L3 edge from 13423.2 to 13419 eV is observed (Fig. 5). This corresponds to reduction of Bi^{3+} to metallic Bi^0, more specifically: $3Li + BiVO_4 \rightarrow Bi + Li_3VO_4$. In the capacity range 280 - 510 mAh g^{-1} corresponding to the voltage plateau at 1.0 V, the Bi L3 edge remains relatively constant. This strongly suggests that the capacity in this voltage range is due to reduction of vanadium from V^{5+} to V^{3+}. The theoretical capacity for a two electron reduction of $BiVO_4$ is 166 mAh g^{-1}, whereas the extension of the Bi L3-edge plateau corrresponds to about 230 mAh g^{-1}, see Fig. 5. This is in relatively good agreement with expectations for the V^{5+}/V^{3+} redox couple (166 mAh g^{-1}), but could indicate an reduction of vanadium even to V^{2+} (249 mAh g^{-1} for the V^{5+}/V^{2+} redox couple). Unfortunately, the V K edge could not be investigated in transmission geometry due to insufficient sample signal caused by large absorption from the separator and electrolyte in the low energy range (V K edge 5465 eV).

The continuous shift of the Bi L3 edge flattens out at 13415.6 eV (corresponding capacity of 920 mAh g^{-1}, Fig. 5) and suggests a further reduction of metallic bismuth. This additional capacity of 410 mAh g^{-1} fits well with a 5 electron reduction (theoretical capacity of 414 mAh g^{-1}) of Bi and V^{3+}. This clearly supports the two step reduction $3Li + Bi \rightarrow 2Li + LiBi \rightarrow Li_3Bi$ (theoretical capacity of 256 mAh g^{-1}) with an edge shift of Bi from 13419 to 13415.6 eV. This is in good agreement with our previous report on the reduction to bismuth in Na_3Bi (Bi^{3-}).[25] The remaining additional capacity might come from further reduction of vanadium, as reported by Liang *et al.* and mentioned above.[26] Some additional capacity may be due to carbon, specifically at voltages below 0.2 V.[27] On charging (Fig. 4), the Bi L3 edge shifts back to about 13419 eV, indicating oxidation of Bi^{3-} to metallic Bi^0. During the 2nd discharge the Bi L3 edge shifts again reversibly to 13415.6 eV.

From the *operando* XANES data and the dQ dV^{-1} curves (Fig. 3) we conclude that subsequent to the initial discharge, Bi is cycling reversibly according to the scheme $3Li + Bi \leftrightarrow LiBi + 2Li \leftrightarrow Li_3Bi$. We note that the Bi L3 edge remains unchanged at the end of the 1st charge (above about 495 mAh g^{-1}) and at the beginning of the 2nd discharge (below 210 mAh g^{-1}). We attribute this to the aforementioned V^{5+}/V^{3+} redox pair and the corresponding reaction; $2Li + Li_3VO_4 \leftrightarrow Li + Li_4VO_4 \leftrightarrow Li_5VO_4$. It is evident that Bi is not oxidized back to Bi^{3+}, confirming the non-reversibility of the initial conversion reaction.

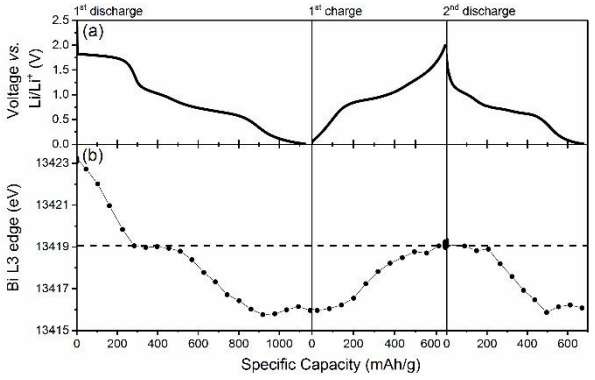

Fig. 5. (a) Voltage vs. Li/Li^+ (V) and (b) Bi L3 edge position (eV) as a function of specific capacity (mAh g^{-1}) for 1st discharge (left), 1st charge (middle) and 2nd discharge (right). Filled circles denotes the capacity at which XANES data were collected.

Energetics of reactions

DFT simulations provide additional insight to the findings from *operando* experiments, especially with respect to the x-ray amorphous phases. The energetics of possible reactions in the investigated Li – $BiVO_4$ system are summarized in Table 1 along with values for electron transfer and theoretical capacities. The assumed first conversion stage $3Li + BiVO_4 \rightarrow Bi + Li_3VO_4$ is highly favoured energetically, -686 kJ mol^{-1}, and in line with the three electron transfer plateau at about 1.75 V in Fig. 5. *Operando* SXRD shows a complete loss of long range order during the conversion reaction and metallic Bi^0 appears subsequently. Based on Table 1, no other pathway appears likely for this first stage.

According to the XANES data, the second capacity window after the formation of $Bi + Li_3VO_4$ does not involve any reduction of Bi. Hence, the reduction will expectedly involve vanadium. The galvanostatic data suggests an exchange of two electrons. We have tentatively ascribed this to V^{5+}/V^{3+}, however, as seen from the energy calculations, a first step V^{5+}/V^{4+} appears possible, although the reaction is only weakly exothermic (-17 kJ/mol). However, a reduction second step V^{4+}/V^{3+} within the frame of the Li_3VO_4 atomic arrangement appears less likely (+306 kJ mol^{-1}). Hence, one may speculate whether the amorphization provides a different local structural arrangement for the Li-V-O phase. Answers may possibly be obtained via PDF based analysis of non-crystalline products.28

The initial amorphization of BiVO4 is the main reason for capacity loss in this system. However, subsequent to first cycle, the performance is very good. It would still be of interest to synthesise a pre-lithiated anode material based on $BiVO_4$ with the goal of avoiding the initial conversion.

In accordance with operando SXRD, the alloying of Bi with Li takes place in two distinct steps, first to LiBi (-73 kJ mol-1) and then to Li3Bi (-133 kJ mol-1). As seen from the dQ dV-1 plot, Fig. 3, two cathodic peaks, at about 0.73 and 0.62 V, are related to these two alloying reactions.

Table 1. Suggested reaction steps with calculated enthalpies, number of electrons transferred and theoretical capacity (mAh g^{-1}). Redox active cations/metals are marked in bold.

	Reaction steps	Reaction enthalpy		Electron transfer	Theoretical capacity
1	$3Li + \mathbf{Bi}VO_4 \rightarrow \mathbf{Bi} + Li_3VO_4$	-7.108 eV	-686 kJ mol^{-1}	3	248 mAh g^{-1}
2	$Li+Li_3\mathbf{V}O_4 \rightarrow Li_4\mathbf{V}O_4$	-0.171 eV	-17 kJ/mol^{-1}	1	83 mAh g^{-1}
3	$Li+Li_4\mathbf{V}O_4 \rightarrow Li_5\mathbf{V}O_4$	3.174 eV	306 kJ mol^{-1}	1	83 mAh g^{-1}
4	$Li+\mathbf{Bi} \rightarrow Li\mathbf{Bi}$	-0.752 eV	-73 kJ mol^{-1}	1	83 mAh g^{-1}
5	$2Li+Li\mathbf{Bi} \rightarrow Li_3\mathbf{Bi}$	-1.374 eV	-133 kJ mol^{-1}	2	166 mAh g^{-1}

Conclusions

We report on the electrochemical performance of $BiVO_4$ as a lithium ion battery anode. We demonstrate a specific charge capacity of 485 mAh g^{-1} after 50 cycles (graphite 372 mAh g^{-1} theoretical capacity). The use of *operando* quasi simultaneous synchrotron x-ray diffraction and absorption in combination with galvanostatic cycling, including dQ dV^{-1} plots, allowed us to pinpoint the conversion reaction of $BiVO_4$ during the initial lithiation with a subsequent reversible cycling of $3Li + Bi \leftrightarrow LiBi + 2Li \leftrightarrow Li_3Bi$. We provide indirect proof of the reversibility of V^{5+}/V^{3+} redox couple. Our interpretation of the reaction mechanisms is supported by DFT reaction energy calculations.

Conflicts of interest

There are no conflicts to declare.

Acknowledgements

We thank Matthias Hermann for fruitful discussions and participation in synchrotron experiments. We thank Davis S. Wragg for discussions. We thank Hermann Emerich and Wouter van Beek at Swiss-Norwegian Beamlines, BM31, ESRF, for assistance. The authors gratefully acknowledge the Research Council of Norway (Grant agreement no.: Nano-MILIB, 143732) for financial support. PV acknowledges the Research Council of Norway for providing computer time (under the project number NN2875k) at the Norwegian supercomputer facilities.

References

1. C. P. Sandhya, B. John and C. Gouri, *Ionics*, 2014, 20, 601-620.
2. Y. Zhao, X. Li, B. Yan, D. Xiong, D. Li, S. Lawes and X. Sun, *Advanced Energy Materials*, 2016, 6, 1502175.
3. K. Cao, T. Jin, L. Yang and L. Jiao, *Materials Chemistry Frontiers*, 2017, 1, 2213-2242.
4. M. Zheng, H. Tang, L. Li, Q. Hu, L. Zhang, H. Xue and H. Pang, *Advanced Science*, 2018, 5, 1700592.
5. C. Yuan, H. B. Wu, Y. Xie and X. W. Lou, *Angewandte Chemie International Edition*, 2014, 53, 1488-1504.
6. F. Huang, Z. Yuan, H. Zhan, Y. Zhou and J. Sun, *Materials Letters*, 2003, 57, 3341-3345.
7. D. Dubal, D. Patil, S. Patil, N. R. Munirathnam and P. Gomez-Romero, *ChemSusChem*, 2017, DOI: 10.1002/cssc.201701483.
8. D. P. Dubal, K. Jayaramulu, R. Zboril, R. A. Fischer and P. Gomez-Romero, *Journal of Materials Chemistry A*, 2018, 6, 6096-6106.
9. J. Sottmann, M. Herrmann, P. Vajeeston, A. Ruud, C. Drathen, H. Emerich, D. Wragg and H. Fjellvåg, *Chemistry of Materials*, 2017, 29, 2803-2810.
10. R. Muruganantham and W. R. Liu, *ChemistrySelect*, 2017, 2, 8187-8195.
11. P. P. R. M. L. Harks, F. M. Mulder and P. H. L. Notten, *J. Power Sources*, 2015, 288, 92-105.
12. M. Morcrette, Y. Chabre, G. Vaughan, G. Amatucci, J. B. Leriche, S. Patoux, C. Masquelier and J. M. Tarascon, *Electrochimica Acta*, 2002, 47, 3137-3149.
13. A. M. Tripathi, W.-N. Su and B. J. Hwang, *Chemical Society Reviews*, 2018, 47, 736-851.
14. A. Bruker, *Bruker AXS, Karlsruhe, Germany*, 2009.
15. B. Ravel and M. Newville, *Journal of Synchrotron Radiation*, 2005, 12, 537-541.
16. J. Sottmann, R. Homs-Regojo, D. S. Wragg, H. Fjellvag, S. Margadonna and H. Emerich, *Journal of Applied Crystallography*, 2016, 49, 1972-1981.
17. G. Kresse and J. Furthmüller, *Phys. Rev. B*, 1996, 54, 11169-11186.
18. G. Kresse and J. Furthmüller, *Comput. Mater. Sci.*, 1996, 6, 15-50.
19. J. P. Perdew, K. Burke and M. Ernzerhof, *Phys. Rev. Lett.*, 1996, 77, 3865.
20. https://www.fiz-karlsruhe.de/de/leistungen/kristallographie/icsd.html, Inorganic Crystal Structure Database (ICSD)
21. I. A. Courtney, J. S. Tse, O. Mao, J. Hafner and J. R. Dahn, *Phys. Rev. B*, 1998, 58, 15583-15588.
22. K. Momma and F. Izumi, *Journal of Applied Crystallography*, 2011, 44.
23. W. Xianming, T. Nishina and I. Uchida, *Journal of Power Sources*, 2002, 104, 90-96.
24. C. Liao, Q. Zhang, T. Zhai, H. Li and H. Zhou, *Energy Storage Materials*, 2017, 7, 17-31.
25. J. Sottmann, M. Herrmann, P. Vajeeston, Y. Hu, A. Ruud, C. Drathen, H. Emerich, H. Fjellvåg and D. Wragg, *Chemistry of Materials*, 2016, 28, 2750-2756.
26. Z. Liang, Z. Lin, Y. Zhao, Y. Dong, Q. Kuang, X. Lin, X. Liu and D. Yan, *Journal of Power Sources*, 2015, 274, 345-354.
27. F. Legrain, J. Sottmann, K. Kotsis, S. Gorantla, S. Sartori and S. Manzhos, *The Journal of Physical Chemistry C*, 2015, 119, 13496-13501.
28. J. Sottmann, M. Di Michiel, H. Fjellvåg, L. Malavasi, S. Margadonna, P. Vajeeston, G. B. M. Vaughan and D. S. Wragg, *Angewandte Chemie International Edition*, 2017, 56, 11385-11389.